ACS APPLIED MATERIALS & INTERFACES

Research Article

Cite This: ACS Appl. Mater. Interfaces XXXX, XXX, XXX−XXX

www.acsami.org

Self-Cleaning Porous Surfaces for Dry Condensation

Kang Liu,[†,‡,∥] Zhi Huang,[§,∥] Ali Hemmatifar,[‡] Diego I. Oyarzun,[‡] Jun Zhou,[†] and Juan G. Santiago*[,‡]

[†]Wuhan National Laboratory for Optoelectronics, Huazhong University of Science and Technology, Wuhan 430074, China

[‡]Department of Mechanical Engineering, Stanford University Stanford, 440 Escondido Mall, Stanford, California 94305, United States

[§]School of Energy & Environmental Engineering, University of Science and Technology Beijing, Beijing 100083, China

Supporting Information

ABSTRACT: Efficient water removal from a cool surface during condensation is critically important to the enhancement of a variety of heat transfer applications. Previous work has focused on the fabrication of superhydrophobic surfaces which promote water droplets and removal via droplet shedding or jumping. Here, we report a novel strategy with a droplet self-cleaning surface which spontaneously transports all of the droplets from the condensation surface to the back side. We fabricate the self-cleaning surface by simply tailoring the wettability of the two sides of a porous membrane and demonstrate that the hydrophobic side is effective in clearing off droplets of a wide range of diameters. Even during rapid impingement of droplets smaller than 10 μm, this surface remains dry. We further demonstrate a "dry condensation" process wherein a surface undergoing rapid condensation is maintained free of droplets. This minimizes the essential thermal resistance of the process, and we estimate a twofold increase in condensation rate compared with a simple copper surface under the same conditions. Our method is tailorable, extendable to a wide range of materials and geometries, and shows great potential for a broad range of condensation processes.

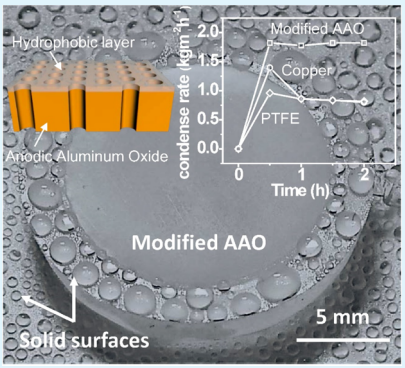

KEYWORDS: *self-cleaning, condensation, water harvest, porous surface, microfluidics*

多孔膜两面润湿性调节

清洁效果作用于疏水面

Condensation is an ubiquitous process in nature[1,2] and has a dominant influence on the performance of water recycle, energy generation, and heat transfer in a variety of industrial applications, including phase-change-based desalination,[3−6] water harvesting from air,[7] thermal power plant, and air conditioning.[8] In all of these applications, condensation with low thermal resistance is essential to save energy or natural resources. Water film and significant density droplets on a surface can result in high thermal resistance[9] and hinders subsequent condensation. This self-limiting behavior can be disrupted by the rapid and continuous removal of liquid water as it condenses on the surface.[10,11] Traditional strategies employ a hydrophobic surface to maintain dropwise condensation or hydrophilic/hydrophobic pattern to improve the droplet shedding.[10−17] This approach can promote the condensation efficiency by sweeping the droplets with a sufficiently large size. However, this method nevertheless supports some time-averaged density of drops on the surface, limiting heat transfer. An ideal cleaning method should keep the surface clear of drops at all times and maximize the heat transfer coefficient. We have termed this ideal condition "dry condensation".

The key challenge for dry condensation is the ability for fast and spontaneous removal of the condensed water away from the cooling surface. To address this, we here report a droplet self-cleaning surface fabricated from a porous membrane. The surface quickly and spontaneously transports droplets on one surface to the back side, even against a hydrostatic head. We demonstrate that the surface remains observably free of drops even under high flux impingement of droplets from a mist spray or humidifier. We also demonstrate that the surface is observably free of drops for more than 10 h of condensation. The dry condensation surface maintains a condensation rate of 1.9 kg m^{-2} h^{-1} at a surface subcooling of 12 °C relative to the environment; this is two times the value of a copper surface under the same conditions and setup. The results show great potential in a broad range of water-harvesting and phase-change heat transfer applications.

高通量液体撞击的情况下，依然能保持干燥状态

RESULTS AND DISCUSSION

We fabricated the droplet self-cleaning surface with an anodic aluminum oxide (AAO) membrane. The surface has vertically aligned pores of 200 nm in diameter (Figures 1a, S1). The original AAO was hydrophilic with the contact angle of ∼10° (Figure 1b). We modified one side of the membrane to be hydrophobic with a layer of dodecyltrichlorosilane.[18,19] As shown in Figure 1c, the modified surface has a contact angle of 128° and the pores remain open (Figure S1). Even after such a

Received: May 3, 2018
Accepted: July 16, 2018

DOI: 10.1021/acsami.8b07261
ACS Appl. Mater. Interfaces XXXX, XXX, XXX−XXX

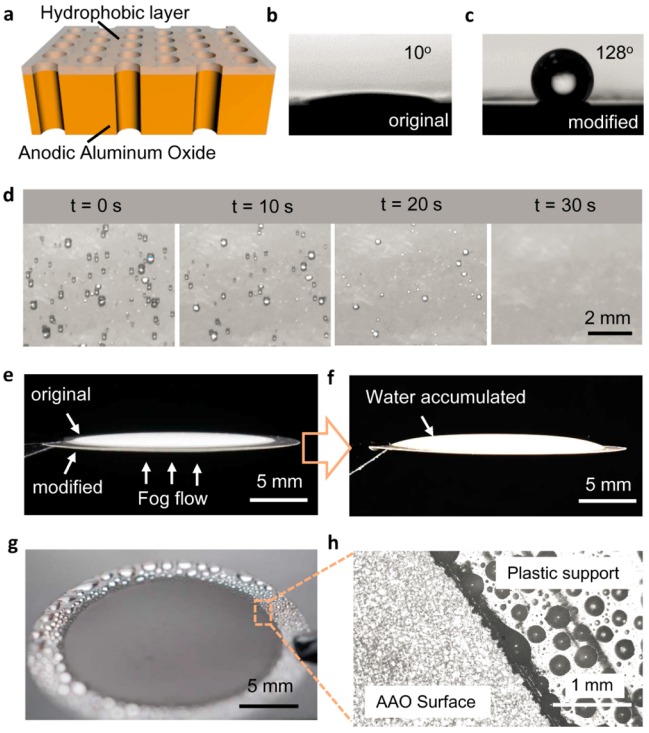

Figure 1. Droplet self-cleaning surface fabricated from an AAO membrane. (a) Schematic of the structure of the modified AAO membrane. (b,c) Contact angle of the original (b) and modified surface (c). (d) Images show the droplets self-cleaning behavior on the surface of the AAO membrane. Droplets of varying volumes are deposited on the surface with a spray. The surface is observably free of liquid water within about 30 s. This phenomenon is repeatable when the hydrophobic side is facing down. (e–f) Images show the surface subjected to a humid fog. (e) Initial state of the experiment setup and (f) final state after being subjected to humid fog for 10 min. Water accumulation was observed on the hydrophilic side of the membrane. (g) Image of the AAO surface from the hydrophobic side. A large number of droplets are visible on the plastic support around the AAO, but the AAO surface is completely clean of visible liquid water. (h) Microscope image shows the sharp contrast between the self-cleaning AAO surface and the plastic supporting frame along the edge of the membrane.

simple treatment, the hydrophobic side of the membrane shows strong droplet self-cleaning capability, even for significantly small droplets with diameters smaller than 10 μm. Figure 1d shows the surface that we prewet the hydrophilic (back) side with water to fill the membrane pores. After this prewetting, we deposited droplets of diameters between about 50 and 260 μm on the hydrophobic (front) side using a spray. All of these droplets vanished within a few seconds (30 s for Figure 1d), leaving the hydrophobic surface clean and dry. Compare this behavior to, for example, a superhydrophobic surface which cannot keep a droplet-free surface for droplets of similar size (see comparison experiments in Figure S2).

We also verified the self-cleaning ability of our surface by subjecting it to a humid fog generated by an ultrasonic humidifier (Figure 1e). The humidifier produces droplets with diameters of about 1 to ~10 μm.[20] The AAO surface again remained dry despite the continuous impingement of small droplets, as shown in Figure 1g,h and Video S1. All of the droplets were spontaneously translocated (transported through membrane) from the hydrophobic side and accumulated at the hydrophilic side (Figure 1f). This transport occurs in a direction opposed by gravity. To demonstrate the robustness and flexibility of this phenomenon, we fabricated and demonstrated a similar function using two other porous materials: a carbon aerogel and nickel oxide.[21] These comparison cases have a pore structure and were subjected to the same surface treatment. The carbon aerogel and nickel oxide showed similar droplet self-cleaning ability to the AAO membrane (see data and discussion around Figure S3).

To further study the origin of this phenomenon, we performed a set of controlled experiment using a system with optical access and precise pore geometry. These experiments included visualization of individual droplets in contact with and translocating through a single pore. We used a 2 mm thick polydimethylsiloxane (PDMS) film as shown in Figure 2a. The PDMS film included a straight pore with

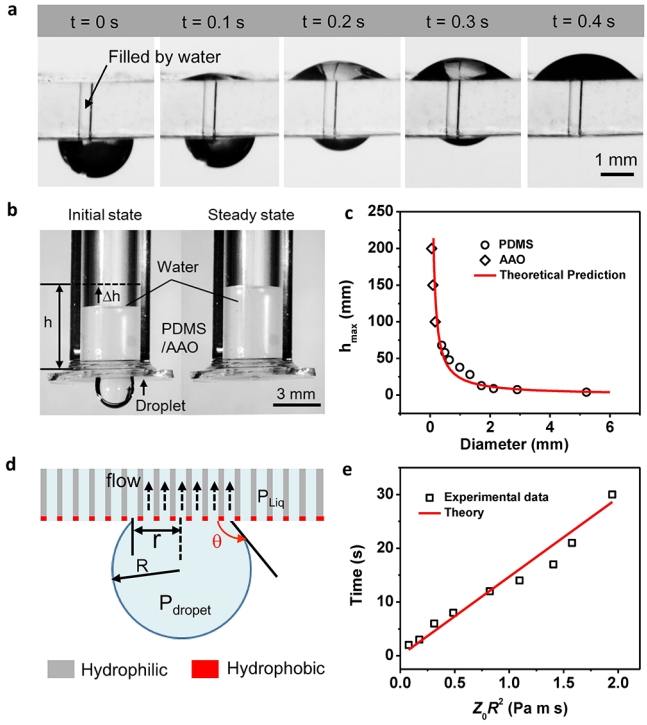

Figure 2. Mechanism of droplet translocation. (a) Sequence of images showing dynamics of a 4 μL droplet transporting from the hydrophobic side of the PDMS film to the hydrophilic side through a single pore. (b) Image shows a droplet transport into the tube and increasing water height. (c) Measurements of the maximum hydrostatic head height that a droplet can overcome as a function of droplet diameter. (d) Schematic of the mechanism for the droplet transport inside the porous film. The droplet air–liquid interface touches no gradient in surface energy, and we hypothesize that Laplace pressure of drop itself is the driving force. (e) Measured droplet translocation times, t_{trans}, on the AAO surface as a function of the product of single-phase membrane pore flow resistance per area and droplet radius squared, Z_0R^2 (symbols). The solid line is an approximate scaling law suggested by our simple model.

circular across section 400 μm in diameter (Figure S4). The pristine PDMS film surface was hydrophobic with the contact angle of 110°. We treated one side of the PDMS film with air plasma for 30 s under the power of 18 W. The air plasma treatment promoted oxygen-containing functional groups on one surface and inside the pore, rendering theses surfaces hydrophilic[22,23] (see Figures S4–S6). After prefilling the pore

液滴与空隙接触、迁移的可视化

亲水侧润湿

DOI: 10.1021/acsami.8b07261
ACS Appl. Mater. Interfaces XXXX, XXX, XXX–XXX

with water, we placed a 2 μL droplet on the hydrophobic side using a standard pipette. The droplet was observed to be transported from the hydrophobic side to the hydrophilic side in about 0.4 s, even against the action of gravity (Figure 2a, Video S2). Here, it is important to note that, for the AAO membrane, we obtained the wettability difference by modifying one side of an original hydrophilic porous material to be hydrophobic. For the PDMS film, on the other hand, we created the wettability difference by treating one side of an original hydrophobic material to be hydrophilic. Despite the difference in approaches and geometry, the two systems show the same droplet self-cleaning behavior. These results indicate that the hydrophobic surface is maintained free of drops, "dry", because droplets are forcibly and rapidly driven toward the hydrophilic side by action of the tailored difference of wettability.

To further quantify how the wettability architecture induces droplet transport, we connected the PDMS film to a plastic tube (inner diameter of 4 mm) above the surface (on the hydrophilic side). We prefilled this tube with roughly 0.045 mL of water. As shown in Figure 2b, droplets nevertheless transport into the tube and increases the height of the water in the tube, overcoming the hydrostatic pressure of the water column in excess of 3.6 mm of hydrostatic height for these pores (Video S3). There have been previous reports showing that wettability gradients can drive droplet transport against gravity.[24−26] However, in our case, the droplet in contact with a prefilled pore (with no intervening air film) has no meniscus in contact with gradients of surface energy. Hence, we conclude surface tension force is not the key driving force here. Instead, we hypothesize the essential driving force in our system is the Laplace pressure sourced by the surface tension of the droplet itself. Such a mechanism is very different from the surface-energy-gradient driving force.[27,28] To support this hypothesis, we measured the maximum height (h_{max}) which droplets of different sizes can overcome. As shown in Figure 2c, h_{max} is significantly higher for smaller droplets, in accordance with Laplace pressure. We estimated the theoretical h_{max} based on balance of surface energy of the droplet and the (gravitational) potential energy in hydrostatic water column as follows

$$S_{Drop}\gamma = V_{Drop}\rho g h_{max} \quad (1)$$

where S_{Drop} and V_{Drop} are the surface area and volume of the droplet. γ and ρ are, respectively, the surface tension and density of water. Substituting the volume and surface area of the droplet with the shape of a spherical dome into eq 1, we obtain

$$h_{max} = \frac{6\gamma}{(2 + \cos\ \theta)(1 - \cos\ \theta)R} \quad (2)$$

where θ is the local contact angle (hydrophobic surface) and R is the radius of the droplet. See further details in section S1 of the Supporting Information. As Figure 2c shows, the estimated h_{max} closely follows the experimental measurements. This strongly supports our hypothesis that Laplace pressure is the essential driving force for the droplet translocation and self-cleaning action. The hydrophobic side is essential in that it creates nonwetting droplet, even for small droplets. This promotes droplets with high Laplace pressure. The hydrophilicity of the far side of the pore presents a region with lower systematic surface energy (considering both droplet and surface). The hydrophilic internal surface of the pore offers a continuous path for fluid flow and helps initiate the process by filling via self wicking of the pore. The physical situation is depicted in Figure 2d.

For these self-cleaning surfaces, a further important parameter is the characteristic translocation time t_{trans} (defined as the time for droplets to translocate and vanish from the hydrophobic surface). We investigated t_{trans} quantitatively for the self-cleaning AAO surfaces. As shown in Figure 2e, the AAO film has measureable t_{trans} values ranging from 2 to 30 s for droplet diameters of 60 to 290 μm, and t_{trans} increases with the droplet diameter. We developed a simple model for this process by considering a volume-flow-rate-limiting viscous resistance as follows

$$\frac{dV_{Drop}}{dt_{trans}} = \frac{A}{Z_0}\Delta p \quad (3)$$

Δp is the driving pressure difference which depends on the diameter of a droplet according to the Young−Laplace equation ($\Delta p = 2\gamma/R$). Z_0 is the flow resistance per area and A is the contact area ($A = \pi r^2$, r is radius of the contact circle, Figure 2d). We performed independent and quantitative experiments to characterize Z_0, which we measured to be 9.54×10^7 Pa s m^{-1} (details in Methods). Assuming a fixed contact angle (θ) during the drop translocation, we then substitute the volume of the droplet to eq 3 and obtain (see more details in section S2, the Supporting Information)

$$t_{trans} = \frac{(2 + \cos\ \theta)(1 - \cos\ \theta)^2}{4 \sin^2 \theta\gamma} Z_0 R^2 \quad (4)$$

Equation 4 suggests that t_{trans} scales as the second power of the radius of the droplet and with flow resistance per area to the first power. We compare this scaling of $t_{trans} \approx Z_0 R^2$ scaling predicted by eq 4 to our experimental data based on high-speed visualization in Figure 2e. The theory has fairly good agreement throughout the range of experiments, with a contact angle value of 118°. This value deviates slightly from the static contact angle value in Figure 1c (128°). We hypothesize this discrepancy is associated with the difference between dynamic and static contact angles and/or the nonhomogeneity in surface energy for different regions of the membrane. In any case, the low translocation times show the ability of the surface to maintain a dry state for applications with small droplets, such as fog collection and condensation. For example, the resulting translocation time for a droplet with a diameter of 10 μm on the modified AAO surface is as low as 35 ms.

As a comparison case, we also investigated the dynamics of translocation for individual droplets through single pores. For these ex situ type experiments, we fabricated single pores of varying diameters into PDMS films exposed to air on both sides. In these experiments, t_{trans} had measurable values ranging from 0.05 to 0.4 s for droplets of 1 to 4 μL volume. As we show in Figure S7 and section S3 of the Supporting Information, the single-pore model and associated experimental data show a scaling of the form $t_{trans} \approx Z_p R^4$ where Z_p is the flow resistance of the single pore. We describe this different scaling and data further in the Supporting Information. As a whole, both the multipore and individual pore experimental results further support our hypothesis that the drop translocation is driven by Laplace pressure of droplets itself and limited by hydraulic resistance through a finite number of accessible pores.

其它文献观点：润湿梯度驱动水的传输

表面张力不是关键的驱动力

本文观点：与表面能驱动力完全不同

疏水面的必要性

弯液面

空隙亲水内

表面为流体流动提供路径

动力源

DOI: 10.1021/acsami.8b07261
ACS Appl. Mater. Interfaces XXXX, XXX, XXX−XXX

Last, we applied the AAO membrane for condensation using the setup depicted in Figure 3a and shown in Figure 3b. The

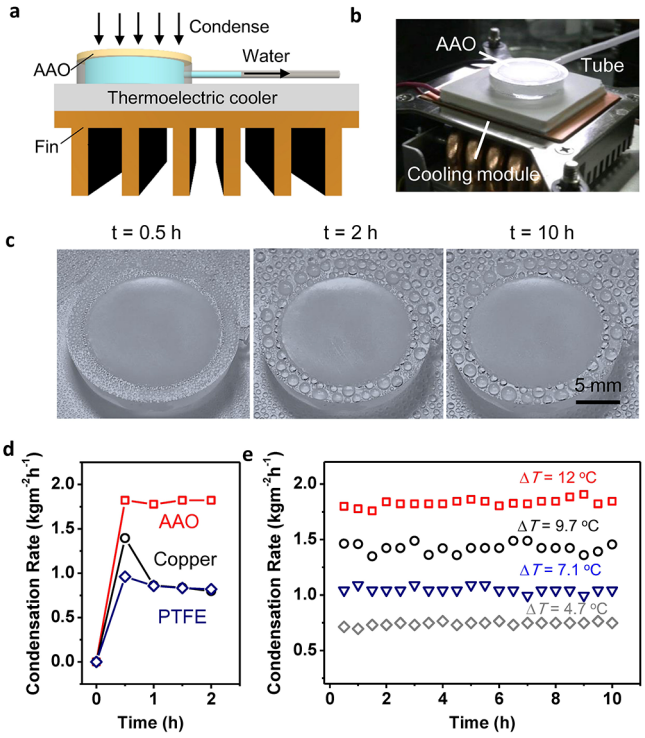

Figure 3. Condensation rate measurements with the self-cleaning "dry condensation" surface. (a) Schematic and (b) image of the setup for condensation measurement. (c) Images of the dry condensation surface of the tailored AAO membrane at 0.5, 2, and 10 h of condensation at fixed temperature. (d) Condensation rates on the surface of AAO membrane, the solid copper, and solid PTFE. The setups for the measurement of copper and PTFE films were placed with an inclination angle of 45° to enhance droplet shedding. All experiments were performed at a room temperature of 24 °C and relative humidity of 55%. (e) Condensation rate of the membrane for surface subcooling ranging from 4.7 to 12 °C.

AAO membrane was placed on top of a glass chamber (diameter of 20 mm and height of 4 mm) and sealed with silica paste. During the experiments, the glass chamber was fully filled with water. We connected a plastic tube to the glass chamber and measured the condensation rate on the AAO surface by the increase of the water in the tube. The temperature of the AAO surface was controlled using a thermoelectric cooler. When we decreased the temperature of the AAO surface to 2 °C (for our room temperature of ~24 °C, the relative humidity is ~55%, and the surface subcooling equals 12 °C), condensation started to occur on the surface of the AAO as well as the nonporous edge around the membrane. We observed dramatic nucleation and growth on this nonporous "frame" around the AAO membrane and the surface of the cooler. However, the surface of the AAO remained dry at all times (Figure 3c, Video S4). Such a dry state is stable for over 10 h. The membrane achieved "dry condensation" through the entire period. For such a dry condensation process, we hypothesize that part of the water condenses directly onto the surface of the outer meniscii of the water-filled pores. We also hypothesize that another portion of water condenses onto the hydrophobic area between pores. The latter condensation forms droplets and which grow to critical sizes before they translocate through the membrane.

We again stress that our dry condensation phenomenon is quite different from condensation on either nonporous hydrophilic or nonporous hydrophobic surfaces. For example, in Figure S8 we show images of two comparison cases: a hydrophilic copper surface and a hydrophobic poly-(tetrafluoroethylene) (PTFE) surface. These images were taken after about 90 min in the same setup as our AAO experiments. The copper surface condensation is initially rapid and efficient, but the rate is quickly limited by a liquid film, as shown in Figure 3d. Similarly, for the hydrophobic surface, the condensation rate decreases with time and is later stabilized (at a lower rate) by periodic droplet shedding. In sharp contrast, our self-cleaning membrane produces a stable dry surface for condensation and can induce a significantly higher condensation rate compared with the solid surface because of the enhanced heat transfer ability. As shown in Figure 3d, the steady-state condensation rate of the modified AAO membrane was ~1.9 kg m^{-2} h^{-1} for the surface subcooling of 12 °C in environmental conditions. The corresponding characteristic heat flux (estimated here simply as the product of condensation rate and latent heat of water) was 1.3 kW m^{-2}, which is approximately two times higher than that of solid copper and hydrophobic PTFE films under the same conditions and setup. Figure 3e shows the performance of the surface under various surface subcooling. In section S4 of the Supporting Information, we present a theoretical estimate of the maximum sustainable condensation rate that our membrane can bear by estimating the flow rate from the Laplace pressure of droplets and the flow resistance of the AAO membrane. Assuming an average droplet radius of 10 μm, the maximum flow rate is 543 kg m^{-2} h^{-1}, a hypothetical value more than two orders of magnitude higher than the value in our experiments. This order-of-magnitude estimate suggests that these membranes have great potential for high condensation rates.

Overall, our results demonstrate that our self-cleaning porous surface can keep itself free of drops or liquid films during both mist impingement and aggressive condensation conditions. We termed the latter phenomenon "dry condensation". The study highlights strong potential for highly efficient condensation under a variety of conditions.

CONCLUSION

In summary, we have shown that a droplet self-cleaning surface can be fabricated by tailoring the hydrophilic/hydrophobic architecture across two sides of a porous membrane. The hydrophobic surface maintains itself observably completely dry when invaded by droplets from the spray or ultrasonic humidifier. We also show a dry condensation state under fairly aggressive condensation conditions with surface subcooling of 12 °C in environment. We offer theories and their comparison with experiments for generated pressure and translocation time. These studies support our hypothesis that the essential driving force in this system is the Laplace pressure of droplets and limited by hydraulic resistance through pores. Compared with the traditional nonporous hydrophilic or hydrophobic surface, the self-cleaning surface maintains a droplet-free surface when exposed to vapor during condensation. This helps minimizing thermal resistance and induces a much higher condensation rate for the same temperature difference (more than two times our comparison solid surface

DOI: 10.1021/acsami.8b07261
ACS Appl. Mater. Interfaces XXXX, XXX, XXX−XXX

cases). In view of the system's simple structure, easy fabrication, and high performance, such a self-cleaning design should have great potential to practical applications including water harvesting from air, phase-change-based desalination, and energy generation and transfer processes.

METHODS

PDMS Film Test. The pristine PDMS film was prepared with the Sylgard 184 Silicone Elastomer Kit from the Dow Corning Corporation. The pore inside the PDMS was produced using a hole-puncher. The PDMS film was then plasma-treated with a plasma cleaner (Harrick Plasma, PDC-32G) for 1 min to render the surface hydrophilic. During this treatment, the other side was protected with polyimide tape and so remained hydrophobic. Droplets of varying diameters were produced with a pipette. The droplet transport was recorded using a microscope equipped with a Thorlabs (DCC1545M) charge-coupled device. Contact angles were measured using a contact angle goniometer (Kino SL200B).

AAO Membrane Test. The AAO membrane was purchased from the Whatman Company. The modified AAO membrane was fabricated by temporarily fixing one side of the AAO membrane to the bottom of a Petri dish with tape and the other side exposed to air. We then placed a droplet of dodecyltrichlorosilane on a surface heated to 110 °C and held the upside down Petri dish over the droplet for 90 s to expose it to the dodecyltrichlorosilane vapor. This treatment modified one side of the AAO membrane, rendering it hydrophobic. Note that the 90 s treatment time also resulted in negligible modification of the interior of pores, so the inner pore surfaces remained hydrophilic. Droplets with a wide range of diameters for the AAO tests were produced with a hand-held spray mist dispenser (Fisher Scientific) and ultrasonic humidifier (Urpower, OD-A001).

Flow Resistance Measurements. The single-phase (liquid) flow resistances through the pores in AAO and PDMS membrane were measured by applying a fixed pressure difference (23 kPa for AAO membrane and 7.7 kPa for PDMS membrane) across the membrane and measuring the flow rates. The pressure difference was provided by a high-pressure gas (nitrogen) cylinder and controlled by a pressure sensor and valve. The flow rate was obtained by recording the decreasing rate of prefilled water in the connecting tube.

Condensation Test. The AAO membrane was placed on top of a glass chamber and sealed using silica paste to prevent vapor from entering through the perimeter and condensing on the cold side of the membrane. A long, horizontal plastic tube was connected to the glass chamber. Before tests, the glass chamber was fully filled with water. Thus, the hydrophilic pores in the membrane are "sealed" with water, so there is negligible transport of vapor through the surface and into the collection chamber. We decreased the temperature of the AAO by a thermoelectric cooler at the bottom of the chamber. Condensation on the AAO surface and translocation of water forced water into the connected tube and increased the length of water inside the tube. This provided a measure of condensation volume and mass flux. The droplets on the plastic support were wiped with a tissue to avoid large droplets falling onto the AAO region in tests of long duration. We measured the condensation rates on the copper and hydrophobic surfaces by placing four individual samples simultaneously on a cold surface with the temperature well-controlled. Four samples were deemed to have the same condensation rate during 2 h of condensation. We successively weighed the mass of condensed water on four samples at the time of 0.5, 1, 1.5, and 2 h, respectively. The rate derived from the mass and time for each sample was taken as the condensation rate at 0.5, 1, 1.5, and 2 h, respectively. Both copper and hydrophobic PTFE films were put on top of the glass chamber during condensation tests as a fair comparison.

ASSOCIATED CONTENT

Supporting Information

The Supporting Information is available free of charge on the ACS Publications website at DOI: 10.1021/acsami.8b07261.

Estimate of the maximum hydrostatic height which can be overcome by the Laplace pressure of droplets; brief theory derivations for scaling droplet translocation times for both the multipore membrane and single-pore system; prediction of the maximum condensation rate supportable by the multipore AAO membrane; scanning electron microscopy images of the AAO membrane; image of droplets from a spray pinned on the superhydrophobic surface; droplet self-cleaning phenomenon on the modified nickel oxide and carbon aerogel; X-ray photoelectron spectroscopy, contact angle, and more characteristics of the PDMS film; and images of the copper and PTFE surfaces during condensation (PDF)

Self-cleaning surface remains dry when subject to a fog from a humidifier (AVI)

Droplet transports from the hydrophobic side to the hydrophilic side in a PDMS membrane (AVI)

Droplet transports into a tube overcoming a certain height of water column (AVI)

Surface condition of the modified AAO during condensation (AVI)

AUTHOR INFORMATION

Corresponding Author

*E-mail: juan.santiago@stanford.edu.

ORCID

Kang Liu: 0000-0002-2781-2581

Ali Hemmatifar: 0000-0001-6716-3144

Jun Zhou: 0000-0003-4799-8165

Juan G. Santiago: 0000-0001-8652-5411

Author Contributions

‖K.L. and Z.H. authors contributed equally to this work.

Notes

The authors declare no competing financial interest.

ACKNOWLEDGMENTS

This work was financially supported by the National Natural Science Foundation of China (51672097, 51606082, 51706016), the China Postdoctoral Science Foundation (2015M570639).

REFERENCES

(1) Parker, A. R.; Lawrence, C. R. Water Capture by a Desert Bettle. *Nature* **2001**, *414*, 33−34.

(2) Zheng, Y.; Bai, H.; Huang, Z.; Tian, X.; Nie, F.-Q.; Zhao, Y.; Zhai, J.; Jiang, L. Directional Water Collection on Wetted Spider Silk. *Nature* **2010**, *463*, 640−643.

(3) Qiblawey, H. M.; Banat, F. Solar Thermal Desalination Technologies. *Desalination* **2008**, *220*, 633−644.

(4) Yang, P.; Liu, K.; Chen, Q.; Li, J.; Duan, J.; Xue, G.; Xu, Z.; Xie, W.; Zhou, J. Solar-driven Simultaneous Steam Production and Electricity Generation from Salinity. *Energy Environ. Sci.* **2017**, *10*, 1923−1927.

(5) Zhou, L.; Tan, Y.; Ji, D.; Zhu, B.; Zhang, P.; Xu, J.; Gan, Q.; Yu, Z.; Zhu, J. Self-assembly of Highly Efficient, Broadband Plasmonic Absorbers for Solar Steam Generation. *Sci. Adv.* **2016**, *2*, e1501227.

DOI: 10.1021/acsami.8b07261
ACS Appl. Mater. Interfaces XXXX, XXX, XXX−XXX

(6) Ghasemi, H.; Ni, G.; Marconnet, A.; Loomis, J.; Yerci, S.; Miljkovic, N.; Chen, G. Solar Steam Generation by Heat Localization. *Nat. Commun.* **2014**, *5*, 4449.
(7) Kim, H.; Yang, S.; Rao, S. R.; Narayanan, S.; Kapustin, E. A.; Furukawa, H.; Umans, A. S.; Yaghi, O. M.; Wang, E. N. Water Harvesting from Air with Metal-organic Frameworks Powered by Natural Sunlight. *Science* **2017**, *356*, 430−434.
(8) Yunus, A.; Michael, A. Thermodynamics: An Engineering Approach; McGraw-Hill, New York, 2006.
(9) Tanasawa, I. Advances in Condensation Heat Transfer. *Adv. Heat Transfer* **1991**, *21*, 55−139.
(10) Miljkovic, N.; Enright, R.; Nam, Y.; Lopez, K.; Dou, N.; Sack, J.; Wang, E. N. Jumping-droplet-enhanced Condensation on Scalable Superhydrophobic Nanostructured Surfaces. *Nano Lett.* **2012**, *13*, 179−187.
(11) Wen, R.; Xu, S.; Ma, X.; Lee, Y.-C.; Yang, R. Three-Dimensional Superhydrophobic Nanowire Networks for Enhancing Condensation Heat Transfer. *Joule* **2017**, *2*, 269.
(12) Miljkovic, N.; Enright, R.; Wang, E. N. Effect of Droplet Morphology on Growth Dynamics and Heat Transfer during Condensation on Superhydrophobic Nanostructured Surfaces. *ACS Nano* **2012**, *6*, 1776−1785.
(13) He, M.; Zhou, X.; Zeng, X.; Cui, D.; Zhang, Q.; Chen, J.; Li, H.; Wang, J.; Cao, Z.; Song, Y.; Jiang, L. Hierarchically Structured Porous Aluminum Surfaces for High-efficient Removal of Condensed Water. *Soft Matter* **2012**, *8*, 6680−6683.
(14) Boreyko, J. B.; Chen, C.-H. Self-propelled Dropwise Condensate on Superhydrophobic Surfaces. *Phys. Rev. Lett.* **2009**, *103*, 184501.
(15) Lo, C.-W.; Wang, C.-C.; Lu, M.-C. Scale Effect on Dropwise Condensation on Superhydrophobic Surfaces. *ACS Appl. Mater. Interfaces* **2014**, *6*, 14353−14359.
(16) Dietz, C.; Rykaczewski, K.; Fedorov, A. G.; Joshi, Y. Visualization of Droplet Departure on a Superhydrophobic Surface and Implications to Heat Transfer Enhancement during Dropwise Condensation. *Appl. Phys. Lett.* **2010**, *97*, 033104.
(17) Narhe, R. D.; Beysens, D. A. Growth Dynamics of Water Drops on a Square-pattern Rough Hydrophobic Surface. *Langmuir* **2007**, *23*, 6486−6489.
(18) Rudich, Y.; Benjamin, I.; Naaman, R.; Thomas, E.; Trakhtenberg, S.; Ussyshkin, R. Wetting of Hydrophobic Organic Surfaces and its Implications to Organic Aerosols in the Atmosphere. *J. Phys. Chem. A* **2000**, *104*, 5238−5245.
(19) Han, X.; Wang, L.; Li, J.; Zhan, X.; Chen, J.; Yang, J. Tuning the Hydrophobicity of ZSM-5 Zeolites by Surface Silanization using Alkyltrichlorosilane. *Appl. Surf. Sci.* **2011**, *257*, 9525−9531.
(20) Rodes, C.; Smith, T.; Crouse, R.; Ramachandran, G. Measurements of the Size Distribution of Aerosols Produced by Ultrasonic Humidification. *Aerosol. Sci. Technol.* **1990**, *13*, 220−229.
(21) Zhang, X.; Kan, W.; Jiang, H.; Chen, Y.; Cheng, T.; Jiang, H.; Hu, X. Capillary-driven Low Grade Heat Desalination. *Desalination* **2017**, *410*, 10−18.
(22) Xue, G.; Xu, Y.; Ding, T.; Li, J.; Yin, J.; Fei, W.; Cao, Y.; Yu, J.; Yuan, L.; Gong, L.; Chen, J.; Deng, S.; Zhou, J.; Guo, W. Water-evaporation-induced Electricity with Nanostructured Carbon Materials. *Nat. Nanotechnol.* **2017**, *12*, 317−321.
(23) Lawton, R. A.; Price, C. R.; Runge, A. F.; Doherty, W. J.; Saavedra, S. S. Air Plasma Treatment of Submicron Thick PDMS Polymer Films: Effect of Oxidation Time and Storage Conditions. *Colloids Surf., A* **2005**, *253*, 213−215.
(24) Chaudhury, M. K.; Whitesides, G. M. How to Make Water Run Uphill. *Science* **1992**, *256*, 1539−1541.
(25) Duvivier, D.; Blake, T. D.; De Coninck, J. Toward a Predictive Theory of Wetting Dynamics. *Langmuir* **2013**, *29*, 10132−10140.
(26) Subramanian, R. S.; Moumen, N.; McLaughlin, J. B. Motion of a Drop on a Solid Surface Due to a Wettability Gradient. *Langmuir* **2005**, *21*, 11844−11849.
(27) Cao, M.; Li, K.; Dong, Z.; Yu, C.; Yang, S.; Song, C.; Liu, K.; Jiang, L. Superhydrophobic "Pump": Continuous and Spontaneous Antigravity Water Delivery. *Adv. Funct. Mater.* **2015**, *25*, 4114−4119.
(28) Huang, S.; Song, J.; Lu, Y.; Lv, C.; Zheng, H.; Liu, X.; Jin, Z.; Zhao, D.; Carmalt, C. J.; Parkin, I. P. Power-free Water Pump Based on a Superhydrophobic surface: Generation of a Mushroom-like jet and Anti-gravity Long-distance Transport. *J. Mater. Chem. A* **2016**, *4*, 13771−13777.

DOI: 10.1021/acsami.8b07261
ACS Appl. Mater. Interfaces XXXX, XXX, XXX−XXX